Photochemistry and Photobiology, 20**, **: *–*

Ultrasensitive Measurements of Microbial Rhodopsin Photocycles Using Photochromic FRET

Halil Bayraktar[1], Alexander P. Fields[2], Joel M. Kralj[1], John L. Spudich[3], Kenneth J. Rothschild[4] and Adam E. Cohen*[1,5]

[1]Department of Chemistry and Chemical Biology, Harvard University, Cambridge, MA
[2]Graduate Program in Biophysics, Harvard University, Cambridge, MA
[3]Department of Biochemistry and Molecular Biology, Center for Membrane Biology, The University of Texas Health Science Center, Houston, TX
[4]Department of Physics and Photonics Center, Boston University, Boston, MA
[5]Department of Physics, Harvard University, Cambridge, MA

Received 12 July 2011, accepted 27 September 2011, DOI: 10.1111/j.1751-1097.2011.01011.x

ABSTRACT

Microbial rhodopsins are an important class of light-activated transmembrane proteins whose function is typically studied on bulk samples. Herein, we apply photochromic fluorescence resonance energy transfer to investigate the dynamics of these proteins with sensitivity approaching the single-molecule limit. The brightness of a covalently linked organic fluorophore is modulated by changes in the absorption spectrum of the endogenous retinal chromophore that occur as the molecule undergoes a light-activated photocycle. We studied the photocycles of blue-absorbing proteorhodopsin and sensory rhodopsin II (SRII). Clusters of 2–3 molecules of SRII clearly showed a light-induced photocycle. Single molecules of SRII showed a photocycle upon signal averaging over several illumination cycles.

INTRODUCTION

Microbial rhodopsins are a large family of light-sensitive seven-helix transmembrane proteins found in archaea (*e.g.* bacteriorhodopsin, sensory rhodopsin II), bacteria (*e.g.* proteorhodopsins, Anabaena sensory rhodopsin) and eukaryotes (*e.g.* algal and fungal rhodopsins) (1,2). These proteins mediate a variety of functions in their hosts, including serving as phototaxis receptors in archaea, signaling by protein–protein interaction (sensory rhodopsins I and II); and in algal phototaxis signaling by light-gated channel activity (channelrhodopsins-1 and -2). They also serve as proton pumps (proteorhodopsins and bacteriorhodopsin), and chloride pumps (halorhodopsin) (3–6). The proton-pumping homologues make a significant contribution to solar energy input into the biosphere (7,8).

Transient absorption, resonance Raman, and FTIR spectroscopies provide exquisitely detailed information on the molecular motions associated with the photocycle (9). These measurements are typically performed at the bulk level, on membrane preparations (10), vesicles (11), films (12), or purified protein in detergent micelles. However, the dynamics of the protein may be significantly different when the protein is in a living cell, due to interactions with other proteins, or, most significantly, due to the presence of a membrane potential. A membrane potential tilts the potential energy surfaces of protons and charged residues, and may thereby dramatically alter the conformation and dynamics. One would like to probe the photocycle in an intact cell or in a single vesicle, with simultaneous measurement or control of the transmembrane voltage by patch clamp technique.

Recently, microbial rhodopsins were introduced as a means to monitor membrane potential in bacteria (13) and neurons (14), with submicron spatial resolution, submillisecond temporal resolution, and millivolt-level precision. These voltage indicators function by using the transmembrane potential to induce a color-shifting transition in the protein. Rhodopsin-based voltage indicators led to the discovery of electrical spiking in single bacterial cells (13), and the first movies of action potentials propagating through single mammalian neurons (14).

A key challenge in using microbial rhodopsins as voltage indicators is to find a sufficiently sensitive spectroscopic readout. Absorption measurements lack sensitivity to detect color changes in a single cell. Endogenous fluorescence of the retinal is also sensitive to voltage and is currently the preferred approach to rhodopsin-based optical voltage measurements. However, the endogenous fluorescence of retinal is dim, so shot noise limits the temporal resolution and sensitivity. An alternative readout of the spectroscopic state of microbial rhodopsins would greatly expand the scope of applications of this new class of voltage sensors. Herein, we describe an ultrasensitive fluorescence readout of the progress through the photocycle that can be performed on samples as small as a few molecules. When applied to rhodopsin-based voltage indicators, this technique may enable faster and more sensitive optical voltage measurements.

All rhodopsins contain a retinylidene chromophore covalently linked *via* a Schiff base to the ε-amino group of a lysine in the protein core (15). Absorption of a photon by the retinal initiates a photocycle in which the protein undergoes a complex series of thermally driven conformational transitions before returning to its initial state (6,16). Herein, we focus on two microbial rhodopsins, blue-absorbing proteorhodopsin (BPR) and sensory rhodopsin II (SRII), with markedly

*Corresponding author email: cohen@chemistry.harvard.edu (Adam Cohen)

different photocycles (Figure S1 in Supporting Information). Upon photoexcitation, BPR undergoes a series of fast transitions (< 5 ms) to a long-lived *O* state, which then relaxes to the unphotolyzed state over hundreds of milliseconds. Upon photoexcitation, SRII undergoes a series of fast transitions to a long-lived *M* state, which then slowly relaxes to *O*, which slowly relaxes to the unphotolyzed state.

Fluorescence resonance energy transfer (FRET) provides a powerful tool for studying macromolecular dynamics (17). The rate of energy transfer is proportional to the inverse sixth power of the separation between donor and acceptor. Hence, in its typical application, FRET is used as a proxy for the spatial separation of donor and acceptor fluorophores. However, the rate of FRET also depends on the spectral separation of the emission of the donor and the absorption of the acceptor, suggesting that FRET can be used to probe spectral shifts in a possibly nonfluorescent acceptor, *i.e.* photochromic FRET (pcFRET) (18,19). The molecular movements associated with the photocycle in most microbial rhodopsins are small (as determined by X-ray crystallography and electron spin resonance) (20–23), but the spectral shifts of the retinal absorption wavelength are as large as several 100 nm. Thus, we hypothesized that a fluorescent dye chosen to have an emission spectrum that overlapped with the absorption of a particular intermediate in the photocycle would be selectively quenched as the protein passed through that state. We covalently linked fluorescent dyes to specific residues in BPR and SRII, and measured the time dependence of the fluorescence brightness subsequent to an initial pump pulse.

MATERIALS AND METHODS

Reagents. 1,2-dioleoyl-sn-glycero-3-phosphate (DOPA), 1,2-Dipalmitoyl-sn-glycero-3-phosphocholine (DPPC), *Escherichia coli* polar lipids, and a mini extruder kit were obtained from Avanti Polar Lipids (Alabaster, AL). n-dodecyl-α-maltopyranoside (DDM) was purchased from Anatrace (Santa Clara, CA). Slide-a-lyzer dialysis cassettes were obtained from Thermo-Scientific (Waltham, MA). Alexa 546 maleimide, Alexa 555 maleimide and Alexa 594 maleimide were purchased from Invitrogen (Eugene, OR). Atto 647N maleimide was purchased from Atto-Tec (Siegen, Germany). Biobeads SM-2 were obtained from Bio-Rad (Hercules, CA). All other reagents and chemicals were from VWR (West Chester, PA). All samples were prepared in 20 mM phosphate buffer, 100 mM NaCl at pH 7.0 (PBS) unless otherwise specified. The plasmid encoding BPR was cloned from strain HOT75M4 and contained a native single cysteine residue at position 117 (24). The plasmid encoding SRII was cloned from *Natronomonas pharaonis* strain DSM2160 (25). We introduced mutations S153C or G120C into the SRII plasmid. The *Halobacterium salinarum* membrane lipids were extracted as described previously (24,26).

Purification and labeling. BPR and SRII were expressed in *E. coli* and purified, following reference (27). Briefly, cells were grown in 1 L of LB-type growth medium for 1 h at 37°C. All-*trans* retinal (5 μM) and inducer (IPTG 1 mM for SRII; arabinose 0.04% for BPR) were added and cells were grown for a further 3 h. Cells were harvested by centrifugation and resuspended in 50 mM Tris, 2 mM $MgCl_2$ at pH 7 and sonicated for 5 min. The lysate was centrifuged and the pellet was resuspended in PBS supplemented with 1% DDM. The mixture was homogenized with a glass/teflon Potter Elvehjem homogenizer and centrifuged again. The sample was passed through a Ni-NTA column for purification, and bound protein was eluted with 400 mM imidazole. The imidazole was removed using dialysis against a solution of DDM in PBS. Purified proteins were labeled with maleimide functionalized fluorescent dyes following instructions provided by Invitrogen. Unreacted dye was quenched with excess cysteine and then removed using multiple washes in buffer containing 0.1% DDM in a 10 kDa cutoff centrifugal filter.

Sample preparation. Four mg of DPPC and 1 mg of DOPA in chloroform were mixed in a small vial and dried under N_2 flow for 1 h. The lipids were then resuspended in 1.5 mL of PBS and vortexed until the solution turned a milky white. The heterogeneous lipid dispersion was converted into monodisperse vesicles by passage through a 100 nm nucleopore membrane using a lipid extruder kit. The size of the vesicles was measured to be 180 nm by dynamic light scattering (DynaPro Instruments) (Figure S2). The same procedure was applied for preparing vesicles from *E. coli* polar lipids or from lipids purified from *H. salinarum*.

BioBeads SM2 (0.0180 g) were washed twice with excess PBS and then incubated with the protein and vesicles, under gentle shaking for 5 h at 4°C. The BioBeads gradually removed the DDM detergent, causing the protein to insert into the lipid vesicles. The supernatant containing the vesicles with protein was stored at 4°C.

Fused silica cover slips and microscope slides were cleaned in piranha solution (a highly corrosive 3:1 mixture of concentrated H_2SO_4 and 30% aqueous H_2O_2) and assembled into a flow cell using double-sided tape. The flow cell was filled with 10 μL of sample. For solution-phase measurements, the vesicles were left freely diffusing in the flow cell and imaged far from the flow cell surfaces. For total internal reflection fluorescence (TIRF) measurements, the vesicles were allowed to adsorb onto the fused silica surfaces for 10 min, forming a continuous lipid bilayer. Unadsorbed vesicles were then washed away with clean buffer.

Pump-probe fluorescence and transient absorption spectroscopy. Illumination was provided from either a white light supercontinuum laser equipped with an acousto-optical tunable filter (SC-450-6-AOTF, Fianium Inc., Southampton, England), a solid-state 532 nm laser (CrystaLaser), a blue light emitting diode (Luxeon V Star, Blue, Lambertian, LXHL-LB5C), or a green light emitting diode (Luxeon V Star, Green, Lambertian, LXHL-LM5C). Epifluorescence measurements were performed in an Olympus IX71 inverted fluorescence microscope with a 60× oil immersion objective, numerical aperture 1.45. Fluorescence was collected on an avalanche photodiode detector (Perkin Elmer SPCM AQRH-14; APD) operated in Geiger mode. The time resolution of the pump-probe fluorescence experiments was set by the 50 ms LED excitation pulse. Prism-type TIRF measurements were performed using a 60× water immersion objective, numerical aperture 1.20, and topside illumination through a dove prism. Fluorescence was imaged on an Andor iXon 897 EMCCD camera operated in frame-transfer mode at 50 frames per second. The instrumentation was controlled with custom software (LabVIEW v8.2, National Instruments) and a Field-Programmable Gate Array (FPGA; PCI-7831R National Instruments, Austin, TX). Data were analyzed with MATLAB (The MathWorks, Natick, MA).

Transient absorption spectra of unlabeled proteins in detergent micelles (1% DDM) were collected in a home-built apparatus comprised of the tunable supercontinuum source focused through a sample-loaded cuvette and on to an amplified photodiode (PDA36A, Thorlabs), under the control of custom LabVIEW software. The blue or green LEDs provided the 50 ms excitation pulse, which also set the time resolution. All experiments were performed at room temperature.

RESULTS AND DISCUSSION

BPR

We measured the visible absorption spectra of the ground state of unlabeled BPR in micelles, which had a maximum at 520 nm at pH 7.0 (Fig. 1a). Excitation of the protein with a 50 ms pulse from a green LED (520–540 nm) led to a transient change in the absorption spectrum. We reconstructed the approximate shape of the absorption spectrum of the *O* intermediate of BPR by plotting the magnitude of this transient absorption at a series of wavelengths (Fig. 1a). The absolute extinction coefficient of the *O* intermediate was not determined because the conversion efficiency of the ground → *O* transition was not known. Other intermediates in the photocycle are expected to decay to the *O* state on a much shorter

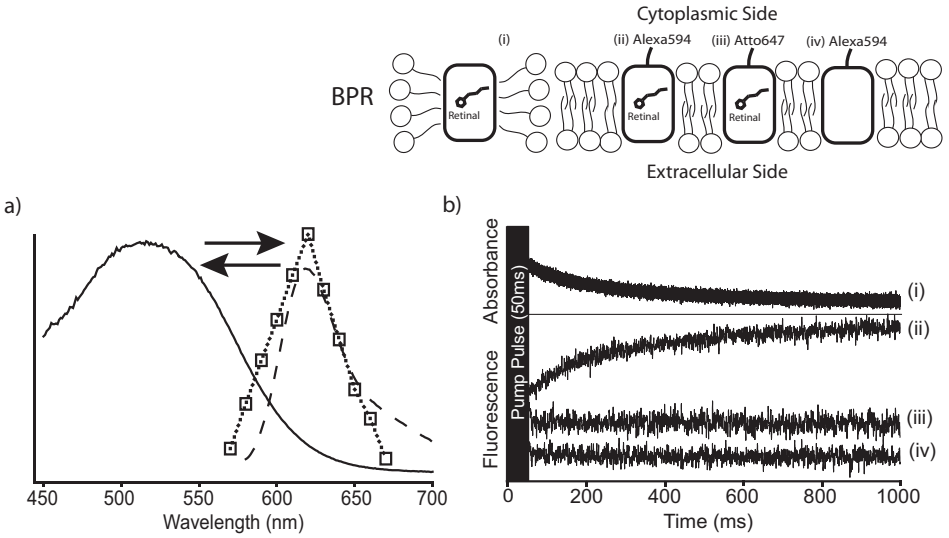

Figure 1. Photochromic FRET probes the photocycle of BPR. (a) Ground state and *O* intermediate absorption spectra of BPR (solid and dotted lines respectively). Emission spectrum of Alexa 594 (dashed line). (b) Transition from *O* to ground state in BPR photocycle. (i) Transient absorption of BPR in DDM probed at 610 nm. Photochromic FRET of (ii) BPR-Alexa 594; (iii) BPR-Atto 647N; and (iv) BPR-Alexa 594 without retinal.

timescale than the 50 ms temporal resolution of this measurement.

Then, we compared the temporal dynamics of the transient absorption at 610 nm (Fig. 1b,i) to the transient fluorescence of a fluorescent dye, Alexa 594, attached at Cys117. This dye was chosen because its emission maximum at 615 nm overlapped with the absorption of the *O* state. Vesicles containing BPR labeled with Alexa 594 were excited with a 50 ms flash from a green LED. The subsequent fluorescence dynamics were probed with excitation at 594 nm (0.5 μW) and detection *via* an APD at wavelengths longer than 610 nm (Fig. 1b). The fluorescence intensity dropped by 8% following the pump pulse, and returned to its steady state value with a time constant of 256 ms (Fig. 1b,ii), matching the timescale of the transient absorption. BPR labeled with Atto 647N, whose emission (λ_{max} = 665 nm) did not overlap with any state in the photocycle, showed no transient fluorescence (Fig. 1b,iii). BPR-Alexa 594 lacking the retinal chromophore also showed no transient fluorescence (Fig. 1b,iv). These experiments were consistent with a model in which the transient fluorescence arose from changes in the spectral overlap of the dye emission with the retinal absorption. The samples were sufficiently optically thin that trivial reabsorption of dye emission by the retinal was not a concern.

Sensory rhodopsin II

Further, we tested our method with SRII, which had a more complex photocycle than BPR at long times, as determined by transient absorption spectroscopy (28). The initial state had an absorption maximum at 490 nm (Fig. 2a). Optical excitation drove the protein to the *M* state (monitored at 400 nm), which had a longer lifetime than in the photocycle of BPR (10,29). The *M* state decayed to the *O* state (λ_{max} = 580 nm), and the *O* state decayed to the initial state. We reconstructed the approximate shape of the absorption spectrum of the *O* intermediate by plotting the maximum transient absorption response at a series of wavelengths following illumination with a 50 ms pulse of light from a blue LED (460–490 nm; Fig. 2a).

To test the hypothesis that pcFRET can probe the kinetics of specific intermediates in the photocycle, we generated two single cysteine mutants of SRII, and labeled each with one of several cysteine-reactive fluorescent dyes. The labeling points were on the cytoplasmic EF loop (S153C) and on the extracellular DE loop (G120C) (Figure S3). Visible transient absorption measurements confirmed that both mutants folded normally and underwent wild-type photocycles. The dyes used were Alexa 546 and 555, both chosen to have emission spectra that overlapped with the *O* intermediate, and Alexa 594, chosen as a negative control because its emission had little overlap with any intermediates in the photocycle. Labeled SRII was reconstituted into vesicles of native lipids from *H. salinarum* and loaded into a fluorescence microscope. The photocycle was initiated using the blue LED (460–490 nm). The dye was excited at 532 nm and fluorescence was collected at wavelengths longer than 550 nm (Alexa 546, 555) or excited at 594 nm and collected at wavelengths longer than 610 nm (Alexa 594). In all cases, the fluorescence excitation power was 0.5 μW, corresponding to an intensity of approximately 25 mW cm^{-2}, and the fluorescence was recorded on an APD.

When attached to the cytoplasmic loop, the dyes Alexa 546 and 555 both showed biphasic transient fluorescence signals of 16% and 8% respectively (Fig. 2b). Similar biphasic transient fluorescence was observed when the extracellular loop was labeled with Alexa 546, although with smaller magnitude (3.5%). The disparity in signal magnitude between the two labeling positions could stem from the fact that the labeling sites were at different distances and angles from the retinal chromophore. Small transient fluorescence (1.5%) was observed when the cytoplasmic loop was labeled with Alexa 594, as expected from the poor spectral overlap between the emission of the dye and the absorption of the *O* state.

The biphasic transient fluorescence of fluorescently labeled SRII was quantitatively explained by a three-state kinetic

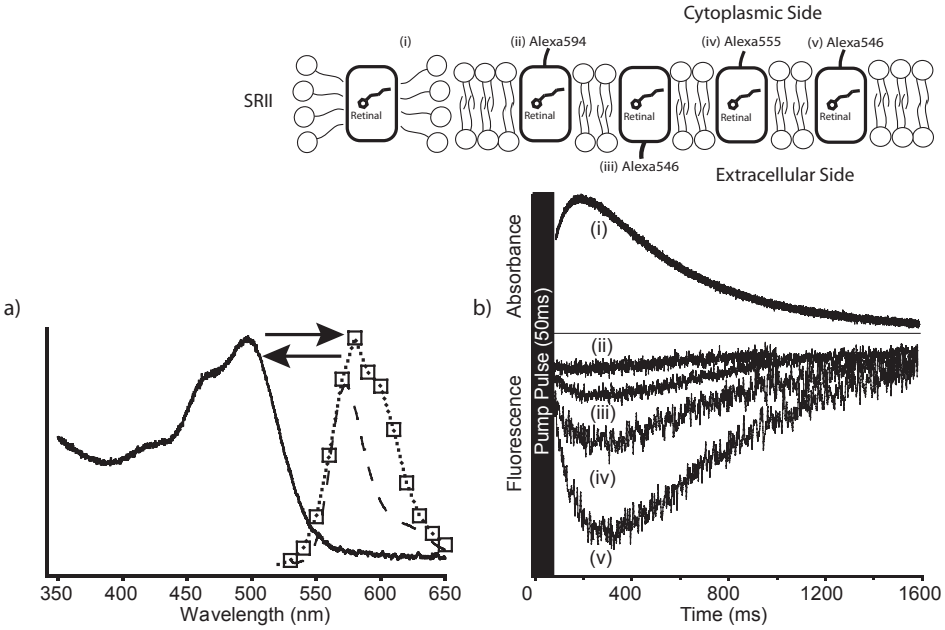

Figure 2. Photochromic FRET measurements of the photocycle in SRII. (a) Unphotolyzed state and *O* state absorption spectra of SRII (solid and dotted lines respectively). Emission spectrum of Alexa 546 (dashed line). (b) Transition from *M* to ground state in SRII photocycle. (i) Transient absorption of SRII in DDM probed at 580 nm. Transient fluorescence of SRII mutants labeled with the dyes and at the locations indicated in the cartoon: (ii) SRII-Alexa 594; (iii) SRII-Alexa 546 (on the extracellular side); (iv) SRII-Alexa 555; and (v) SRII-Alexa 546 (cytoplasmic side).

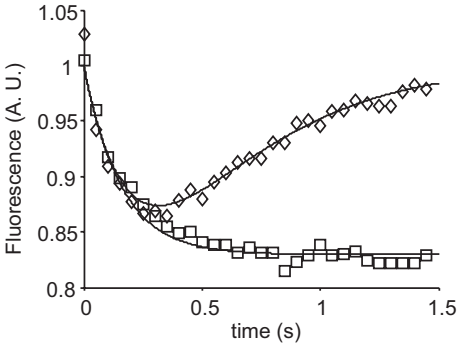

Figure 3. Transient fluorescence of $SRII^{S153C}$-Alexa 546 induced by a 50 ms flash of excitation (diamonds) or step function excitation (squares). Both datasets were fit to the three-state model (Eq. 1) with the same parameters (solid lines).

model comprising the unphotolyzed state, an *M* state, and an *O* state. In the model, only the *O* state quenched the fluorescence, on account of its spectral overlap with the emission of the donor (Fig. 3 and Appendix). The other intermediates in the photocycle were too fast to contribute to the observed dynamics. This model fit the fluorescence dynamics with both brief pulsed pumping of the activating light and with intermittent periods of continuous pumping (see elsewhere in the text).

Four pieces of evidence support the hypothesis that the transient fluorescence signal arose from pcFRET as opposed to from changes in the local environment of the fluorophore: (1) The timecourse of the transient fluorescence was the same for the cytoplasmic and extracellular labeling locations, as expected for pcFRET; (2) The sign of the transient fluorescence was opposite to the sign of the transient absorption, as expected for pcFRET; (3) The timecourse of the transient fluorescence matched the timecourse of transient absorption. In Fig. 2b, the transient fluorescence measured in vesicles was slightly slower than the transient absorption measured in micelles, but when the transient fluorescence was measured in micelles the kinetics matched precisely (Figure S4); and (4) The degree of transient fluorescence correlated with the degree of spectral overlap between the fluorophore and the *O* intermediate. For instance, Alexa 594 showed strong transient fluorescence when attached to BPR, which had good spectral overlap between dye emission and *O* state, but weak transient fluorescence when attached to SRII, which had little spectral overlap between dye emission and *O* state. Nonetheless, it is possible that some of the fluorescence response was due to local environmental changes, as has been observed with fluorescently labeled bacteriorhodopsin (30).

Having established that pcFRET probed the progress through the photocycle, we further studied the behavior of SRII, using the species with the largest transient fluorescence signal, $SRII^{S153C}$-Alexa 546. We searched for conditions, which maximized the magnitude of the transient fluorescence. In the native lipids from *H. salinarum*, the transient fluorescence amplitude was 16%. In vesicles composed of DOPA/DPPC, the signal dropped to 7.6%, and in *E. coli* polar lipids the signal dropped to 4% (Figure S5). Other studies have shown that the folding efficiencies of bacteriorhodopsin and other transmembrane proteins are also sensitive to membrane lipid composition (31–33). Therefore, we used native lipids from *H. salinarum* for microscopic measurements.

Ultrasensitive measurements of pcFRET in SRII

We applied the technique of pcFRET to measure the dynamics of the photocycle in immobilized lipid vesicles containing 1–10

molecules of SRII. In a prelude to these experiments, we characterized the photophysics of SRII under illumination intensities sufficient to detect single molecules. These preliminary experiments were carried out on "quasi-bulk" samples of SRII in surface-immobilized lipid vesicles and showed the existence of a long-lived photoexcited dark state that was not detected under low intensity illumination.

$SRII^{S153C}$-Alexa 546 was introduced into vesicles of native lipid and the vesicles were physically adsorbed onto a fused silica microscope slide and illuminated through a prism-type TIRF setup. Fluorescence was collected through a 60× water immersion objective with a numerical aperture of 1.2 and imaged onto an EMCCD camera.

Although the fluorescence probe wavelength, 532 nm, was redshifted relative to the absorption maximum of the ground state chromophore, at high powers the probe initiated the photocycle. The probe saturated the photocycle at powers greater than approximately 0.1 mW (5 W cm^{-2}). Thus, at high probe powers the blue pump pulse was redundant. Instead, samples were exposed to 2.5 s of light at 532 nm, which served as both probe and continuous pump, followed by a variable period of darkness to allow the protein to relax to the ground state.

Under these conditions, the ensemble-averaged fluorescence showed a monotonic decrease during each probe cycle as in the case of a step function illumination earlier (Fig. 4 top). The fluorescence recovered during each rest cycle, proving that the drop in fluorescence was not due to photobleaching. We prepared a sample of $SRII^{S153C}$-Alexa 546 in which the protein was purified from cells grown in the absence of retinal. This sample showed no transient drop in fluorescence, ruling out dye photophysics as a cause of the dynamics (Fig. 4 bottom), and establishing that the observed dynamics were due to the activity of the protein. These dynamics were fit by the three-state model using the same parameters as for the data taken in bulk with low probe power. These results confirmed that the SRII remained active upon surface immobilization.

Next, we investigated the dynamics of the SRII photocycle as a function of the interval between pump pulses, at a pump power of 3 mW (150 W cm^{-2}) (Fig. 5a). On the basis of three-state model and the data in Fig. 3, one expects more than 99%

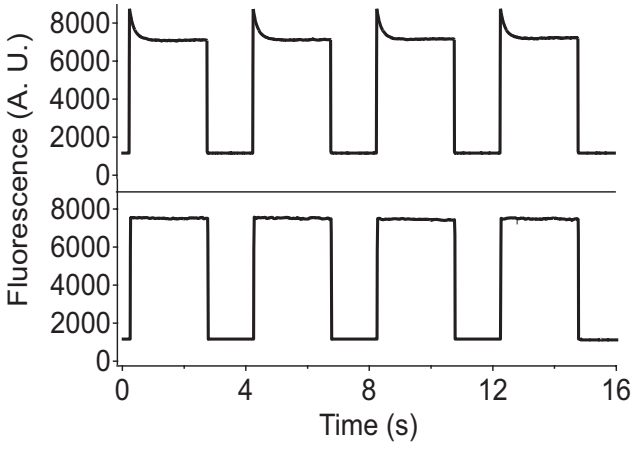

Figure 4. Dynamics of SRII in immobilized lipid vesicles. Ensemble-averaged transient fluorescence of $SRII^{S153C}$-Alexa 546 with retinal (top) and without retinal (bottom). A single beam (1 mW, 532 nm) served as both pump and probe.

of the population to have returned to the unphotolyzed state after a 2 s dark period. Yet, the data showed only a 50% recovery of the transient fluorescence in this interval, with full recovery taking 4.5 s. This discrepancy implied the existence of a state with pcFRET signal indistinguishable from that of the unphotolyzed state.

Further confirmation of the existence of a long-lived state with no pcFRET correlate was obtained from the dependence of the transient fluorescence amplitude on the pump power. The amplitude of the transient fluorescence decreased beyond a critical pump intensity of approximately 5 W cm^{-2} (Fig. 5b). This decrease in signal magnitude was not due to photobleaching: lowering the pump power on the same region of sample led to a recovery of the transient fluorescence. These studies were performed on immobilized vesicles, establishing that the recovery was not due to diffusion. This decreased signal at high power cannot be explained within the three-state model, but could be explained by a long-lived state off pathway in the photocycle. The existence of such an inactive state is similar to a long time decay τ_8 reported by Schmies *et al*. (34). The nature of the inactive state is still unknown, but may be a 9-*cis* photoproduct of *O*, similar to that seen in BR at high illumination power (35).

The unexpected decrease in transient fluorescence amplitude at high probe power presented a challenge for observations of dynamics in single molecules. The peak molecular response occurred at a power of 0.1 mW, but single molecules were undetectably dim at probe powers less than 3 mW. We also desired to count fluorophores by their photobleaching steps, but negligible photobleaching occurred on the timescale of the experiments at powers up to 10 mW. As a compromise, we adopted a two-stage illumination scheme. First, a field of view was illuminated for 2.5 s at 5 mW, followed by 4.5 s of darkness. This pattern was repeated 10 times, and the transient fluorescence was recorded at a frame rate of 50 Hz during each pump cycle. Second, the laser power was increased to 30 mW and photobleaching of each spot was observed under continuous illumination until all the fluorophores had photobleached.

An automated particle-finding algorithm was used to locate individual vesicles in the movies taken at high power (Fig. 6a). For each vesicle, the ratio of its initial intensity to the size of its photobleaching step provided an estimate of the number of fluorophores per vesicle. This algorithm did not always yield an integral number of fluorophores, although the histogram of number of fluorophores per vesicle peaked approximately 1 (Figure S6). The existence of a peak at single-step photobleaching suggested that the proteins in this experiment were monomers. In the native host, SRII and its transducer are comprised of 2:2 heterodimers, and this configuration has been suggested to play a role in signal transduction. The dominance of the monomeric form in our experiments may be due to the absence of the transducer protein HtrII, which is associated with SRII *in vivo* (6,36–39).

Vesicles that showed a single well-resolved photobleaching step during 30 mW illumination were selected for further analysis. These single molecules of SRII fell into two classes based on their behavior in the first part of the experiment. Some showed low-frequency "wandering" of their intensity (Fig. 6b, left), whereas others showed nearly constant intensity (Fig. 6b, right). The transient fluorescence was averaged over

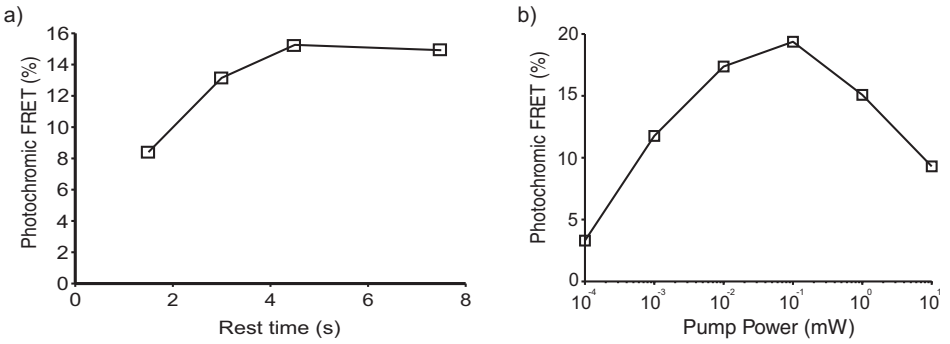

Figure 5. Dependence of photochromic FRET signal of $SRII^{S153C}$-Alexa 546 on (a) rest time between pump pulses and (b) pump power.

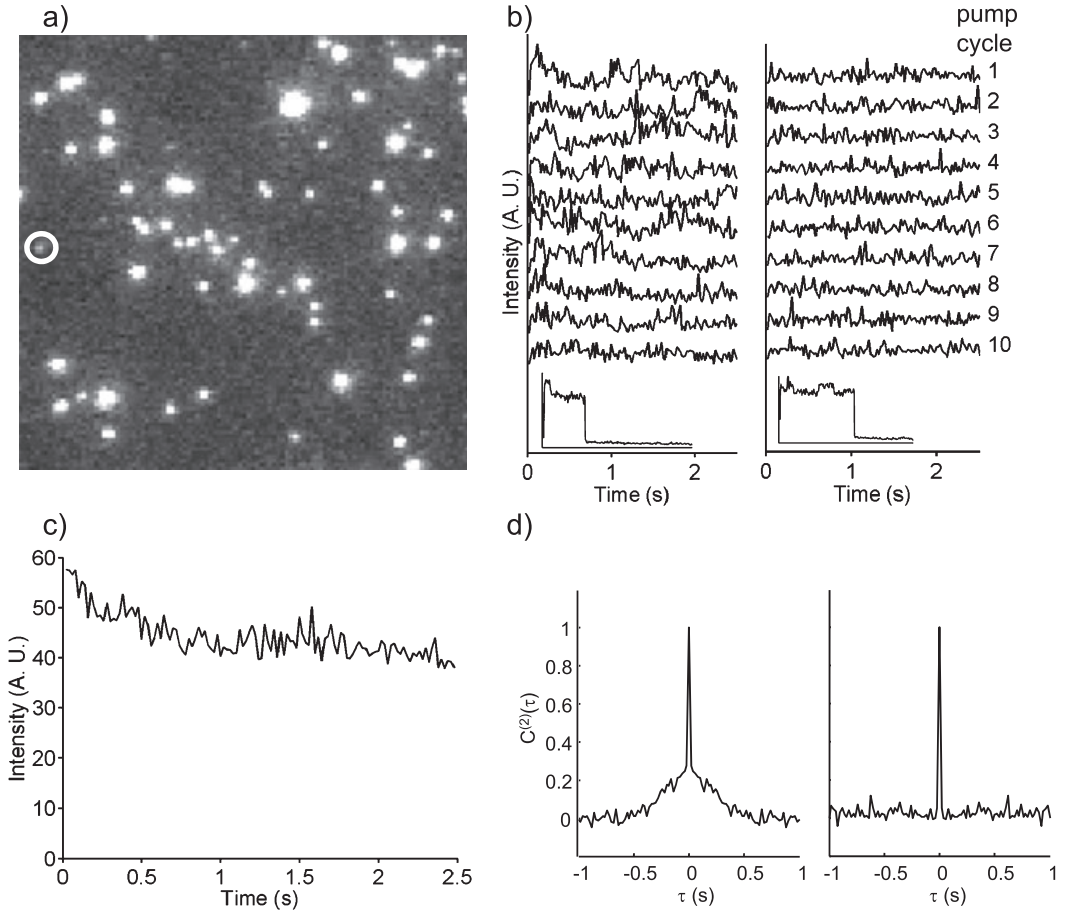

Figure 6. Single-molecule dynamics of SRII in single lipid vesicles. (a) A field of immobilized lipid vesicles containing $SRII^{S153C}$-Alexa 546. A vesicle containing a single molecule of SRII is circled. (b) Fluorescence intensity traces of a single active SRII molecule (left) and a single inactive SRII molecule (right) during 10 consecutive pump cycles. Inset: single-step photobleaching recorded at high power at the end of the experiment. (c) Transient fluorescence signal averaged over 10 pump cycles and nine molecules. (d) Autocorrelation functions of the fluorescence intensity from a single active molecule (left) and a single inactive molecule (right).

10 pump pulses for nine active single molecules, and reproduced the bulk transient fluorescence (Fig. 6c), confirming that the single molecules on the surface were undergoing complete photocycles. Autocorrelation functions of the intensity were calculated from single molecules according to:

$$C^{(2)}(\tau) = \frac{\langle \delta I(t)\delta I(t+\tau)\rangle_t}{\left\langle \delta I(t)^2 \right\rangle_t}$$

Single molecules undergoing active photocycles showed a characteristic relaxation in $C^{(2)}(\tau)$ consistent with the bulk dynamics (Fig. 6d, left). Inactive molecules only showed δ-correlated fluorescence fluctuations, as expected for shot noise (Fig. 6d, right).

On the basis of the three-state model, one would expect to see two fluorescence levels during each pump pulse. At the beginning of each pulse, all molecules should be in the high fluorescence M state. Then the molecules should transition to

the low fluorescence O state, followed by more stochastic transitions between these two states (residence times in the ground state are expected to be undetectably short due to the saturating pump laser). None of the data on single molecules conformed to this two-level fluorescence scheme. Rather, the active molecules tended to show graded transitions between intensity levels. At present it remains unclear whether these transitions reflect hidden substates in the underlying dynamics, or are abrupt transitions masked by noise. Alternatively, there may be rapid equilibrium between M and O spectroscopic states with the balance gradually shifted by slower conformational motions in the protein. The possible entry of molecules into a dark state due to the illumination intensity being increased above the optimal level (Fig. 5) would further obscure the photocycle dynamics.

Photochromic FRET provides an ultrasensitive indicator of the progress of microbial rhodopsins through their photocycle, approaching the level of single molecules in sensitivity. With further advances in dye placement and imaging sensitivity, single-molecule measurements on microbial rhodopsins may become feasible. Even in the absence of single-molecule sensitivity, single-cell measurements of microbial rhodopsin photocycles will yield important information about the dynamics of these proteins in their native biologic context. Although we use organic small-molecule dyes as pcFRET donors, a similar strategy could be envisioned using fluorescent proteins fused to microbial rhodopsins. Such constructs may enable measurements of the photocycle dynamics inside live cells. This strategy is particularly promising as a means to increase the brightness of microbial rhodopsin-based voltage indicators, thereby facilitating optical monitoring of neural activity (13,14).

Acknowledgements—This work was partially supported by NSF Grant CHE-0910824 (H.B., A.P.F., A.E.C.) and the Harvard Center for Brain Science (J.K., H.B.), NIH grant R37GM027750 and chair AU-0009 from the Robert A. Welch Foundation (J.L.S.), and NIH grant R01GM069969 and NSF MRI Award DMR-0821450 (K.J.R.). We thank Xiaowei Zhuang for use of a TIRF microscope.

APPENDIX

Three-state kinetic model of the SRII photocycle

The equations of the model are:

$$\begin{aligned}\frac{d[G]}{dt} &= -k_1 I(t)[G] + k_3[O]\\ \frac{d[M]}{dt} &= k_1 I(t)[G] - k_2[M]\\ \frac{d[O]}{dt} &= k_2[M] - k_3[O]\end{aligned} \quad (1)$$

where $I(t)$ is the time-dependent intensity of the pump beam, k_1, k_2, and k_3 are kinetic parameters, and $[G]$, $[M]$, and $[O]$ are the populations in the unphotolyzed, M, and O states. We considered two time-courses for $I(t)$. In correspondence with the experiment of Fig. 2b, $I(t)$ was approximated as a δ-function that initially placed the entire population in the M state. The ensuing fractional population in the O state was:

$$[O(t)] = \frac{k_2}{k_2 - k_3}(e^{-k_3 t} - e^{-k_2 t}), \quad (2)$$

which increased at short times and decreased to zero at long times.

In another set of experiments, described elsewhere, $I(t)$ was a step function: the pump was turned on and remained on. The fluorescence then showed a monotonic decay, rather than biphasic behavior. Under continuous pumping, molecules that entered the ground state were quickly repumped to the M state. A photostationary state was established between M and O, with negligible population in G. The transient fluorescence measured the relaxation from an initial population of all M to the equilibrium distribution. In the limit of fast, continuous pumping ($I \rightarrow \infty$ in Eq. 1), the population of O followed:

$$[O(t)] = \frac{k_2}{k_2 + k_3}(1 - e^{-(k_2+k_3)t}). \quad (3)$$

In either case, the fluorescence signal reaching the detector was:

$$I_{tot} = I_O[O] + I_G[G] + I_M[M], \quad (4)$$

where I_O, I_G, and I_M, represent the fluorescence intensities of the dye when the protein was in each of the three states. Neither the ground state nor the M state had significant absorption in the emission band of Alexa 546, so we assumed that $I_G = I_M$. Values of k_2, k_3, ands I_O/I_M were adjusted to simultaneously fit Eqs. 2 and 3 to their respective datasets, yielding $k_2 = (396\ \text{ms})^{-1}$, $k_3 = (260\ \text{ms})^{-1}$, and $I_O/I_M = 0.57$. The data and fits are shown in Fig. 3. To extract the parameter k_1, the pump energy was varied by adjusting the duration of the pump pulse from 0.25 to 50 ms. The amplitude of the transient fluorescence showed classical saturation behavior, giving $k_1 = (1\ \text{ms})^{-1}$ for the LED illumination used in these experiments.

SUPPORTING INFORMATION

Additional Supporting Information may be found in the online version of this article:

Figure S1. Schematic photocycles of (a) Blue Proteorhodopsin (BPR) and (b) Sensory rhodopsin II (SRII).

Figure S2. Diameter of DPPC/DOPA vesicles measured using dynamic light scattering (DynaPro Ins., 655 nm, 20 mW). Average size of vesicles was 180 nm.

Figure S3. X-ray structure of sensory rhodopsin II from Protein Data Bank (1JGJ).

Figure S4. Comparison of transient fluorescence (blue) and transient absorption (red) in $SRII^{S153C}$-Alexa 546.

Figure S5. Normalized transient fluorescence of $SRII^{S153C}$-Alexa 546 in vesicles composed of: (1) native lipids (2) DOPA-DPPC and (3) *E. coli* polar lipids.

Figure S6. Histogram of estimated number of molecules of SRII per vesicle.

Please note: Wiley-Blackwell is not responsible for the content or functionality of any supporting information supplied by the authors. Any queries (other than missing material) should be directed to the corresponding author for the article.

REFERENCES

1. Ruiz-Gonzalez, M. X. and I. Marin (2004) New insights into the evolutionary history of type 1 rhodopsins. *J. Mol. Evol.* **58**, 348–358.
2. Sharma, A. K., J. L. Spudich and W. F. Doolittle (2006) Microbial rhodopsins: functional versatility and genetic mobility. *Trends Microbiol.* **14**, 463–469.
3. Fuhrman, J. A., M. S. Schwalbach and U. Stingl (2008) Proteorhodopsins: an array of physiological roles? *Nat. Rev. Microbiol.* **6**, 488–494.
4. Nagel, G., T. Szellas, W. Huhn, S. Kateriya, N. Adeishvili, P. Berthold, D. Ollig, P. Hegemann and E. Bamberg (2003) Channelrhodopsin-2, a directly light-gated cation-selective membrane channel. *Proc. Natl Acad. Sci. USA* **100**, 13940–13945.
5. Kulcsar, A., G. I. Groma, J. K. Lanyi and G. Varo (2000) Characterization of the proton-transporting photocycle of *Pharaonis halorhodopsin*. *Biophys. J.* **79**, 2705–2713.
6. Hoff, W. D., K. H. Jung and J. L. Spudich (1997) Molecular mechanism of photosignaling by archaeal sensory rhodopsins. *Annu. Rev. Biophys. Biomol. Struct.* **26**, 223–258.
7. Moran, M. A. and W. L. Miller (2007) Resourceful heterotrophs make the most of light in the coastal ocean. *Nat. Rev. Microbiol.* **5**, 792–800.
8. Spudich, J. L. (2006) The multitalented microbial sensory rhodopsins. *Trends Microbiol.* **14**, 480–487.
9. Lanyi, J. K. (2004) Bacteriorhodopsin. *Annu. Rev. Physiol.* **66**, 665–688.
10. Wang, W. W., O. A. Sineshchekov, E. N. Spudich and J. L. Spudich (2003) Spectroscopic and photochemical characterization of a deep ocean proteorhodopsin. *J. Biol. Chem.* **278**, 33985–33991.
11. Dioumaev, A. K., J. M. Wang, Z. Balint, G. Varo and J. K. Lanyi (2003) Proton transport by proteorhodopsin requires that the retinal Schiff base counterion Asp-97 be anionic. *Biochemistry* **42**, 6582–6587.
12. Kolodner, P., E. P. Lukashev, Y. C. Ching and D. L. Rousseau (1996) Electric-field-induced Schiff-base deprotonation in D85N mutant bacteriorhodopsin. *Proc. Natl Acad. Sci. USA* **93**, 11618–11621.
13. Kralj, J. M., D. R. Hochbaum, A. D. Douglass and A. E. Cohen (2011) Electrical spiking in *Escherichia coli* probed with a fluorescent voltage indicating protein. *Science* **333**, 345–348.
14. Kralj, J. M., A. D. Douglass, D. R. Hochbaum, D. Maclaurin and A. E. Cohen (2011) Optical recording of action potentials in mammalian neurons using a microbial rhodopsin. To appear in . *Nat. Meth.*
15. Spudich, J. L., C. S. Yang, K. H. Jung and E. N. Spudich (2000) Retinylidene proteins: structures and functions from archaea to humans. *Annu. Rev. Cell Dev. Biol.* **16**, 365–392.
16. Edman, K., A. Royant, P. Nollert, C. A. Maxwell, E. Pebay-Peyroula, J. Navarro, R. Neutze and E. M. Landau (2002) Early structural rearrangements in the photocycle of an integral membrane sensory receptor. *Structure* **10**, 473–482.
17. Lakowicz, J. R. (2006) *Principles of Fluorescence Spectroscopy*, 3rd edn, pp. 443–476. Springer Science, New York.
18. Jares-Erijman, E. A. and T. M. Jovin (2003) FRET imaging. *Nat. Biotechnol.* **21**, 1387–1395.
19. Kuznetsova, S., G. Zauner, T. J. Aartsma, H. Engelkamp, N. Hatzakis, A. E. Rowan, R. J. M. Nolte, P. C. M. Christianen and G. W. Canters (2008) The enzyme mechanism of nitrite reductase studied at single-molecule level. *Proc. Natl Acad. Sci. USA* **105**, 3250–3255.
20. Moukhametzianov, R., J. P. Klare, R. Efremov, C. Baeken, A. Goppner, J. Labahn, M. Engelhard, G. Buldt and V. I. Gordeliy (2006) Development of the signal in sensory rhodopsin and its transfer to the cognate transducer. *Nature* **440**, 115–119.
21. Steinhoff, H. J., A. Savitsky, C. Wegener, M. Pfeiffer, M. Plato and K. Mobius (2000) High-field EPR studies of the structure and conformational changes of site-directed spin labeled bacteriorhodopsin. *Biochim. Biophys. Acta* **1457**, 253–262.
22. Wegener, A. A., I. Chizhov, M. Engelhard and H. J. Steinhoff (2000) Time-resolved detection of transient movement of helix F in spin-labelled pharaonis sensory rhodopsin II. *J. Mol. Biol.* **301**, 881–891.
23. Luecke, H., B. Schobert, J. K. Lanyi, E. N. Spudich and J. L. Spudich (2001) Crystal structure of sensory rhodopsin II at 2.4 angstroms: insights into color tuning and transducer interaction. *Science* **293**, 1499–1503.
24. Bergo, V., E. N. Spudich, K. L. Scott, J. L. Spudich and K. J. Rothschild (2000) FTIR analysis of the SII540 intermediate of sensory rhodopsin II: Asp73 is the Schiff base proton acceptor. *Biochemistry* **39**, 2823–2830.
25. Bergo, V. B., O. A. Sineshchekov, J. M. Kralj, R. Partha, E. N. Spudich, K. J. Rothschild and J. L. Spudich (2009) His-75 in proteorhodopsin, a novel component in light-driven proton translocation by primary pumps. *J. Biol. Chem.* **284**, 2836–2843.
26. Kates, M., S. C. Kushwaha and G. D. Sprott (1982) Lipids of purple membrane from extreme halophiles and of methanogenic bacteria. In *Methods in Enzymology* (Edited by L. Packer), pp. 98–110. Academic Press, New York.
27. Bergo, V., E. N. Spudich, J. L. Spudich and K. J. Rothschild (2003) Conformational changes detected in a sensory rhodopsin II-transducer complex. *J. Biol. Chem.* **278**, 36556–36562.
28. Chizhov, I., G. Schmies, R. Seidel, J. R. Sydor, B. Luttenberg and M. Engelhard (1998) The photophobic receptor from Natronobacterium pharaonis: temperature and pH dependencies of the photocycle of sensory rhodopsin II. *Biophys. J.* **75**, 999–1009.
29. Beja, O., E. N. Spudich, J. L. Spudich, M. Leclers and E. F. Delong (2001) Proteorhodopsin phototrophy in the ocean. *Nature* **411**, 786–789.
30. Alexiev, U., I. Rimke and T. Pohlmann (2003) Elucidation of the nature of the conformational changes of the EF-interhelical loop in bacteriorhodopsin and of the helix VIII on the cytoplasmic surface of bovine rhodopsin: a time-resolved fluorescence depolarization study. *J. Biol. Chem.* **328**, 705–719.
31. Allen, S. J., A. R. Curran, R. H. Templer, W. Meijberg and P. J. Booth (2004) Controlling the folding efficiency of an integral membrane protein. *J. Mol. Biol.* **342**, 1293–1304.
32. Botelho, A. V., N. J. Gibson, R. L. Thurmond, Y. Wang and M. F. Brown (2002) Conformational energetics of rhodopsin modulated by nonlamellar-forming lipids. *Biochemistry* **41**, 6354–6368.
33. Lee, A. G. (2004) How lipids affect the activities of integral membrane proteins. *Biochim. Biophys. Acta* **1666**, 62–87.
34. Schmies, G., B. Luttenberg, I. Chizhov, M. Engelhard, A. Becker and E. Bamberg (2000) Sensory rhodopsin II from the haloalkaliphilic *Natronobacterium pharaonis*: light-activated proton transfer reactions. *Biophys. J.* **78**, 967–976.
35. Popp, A., M. Wolperdinger, N. Hampp, C. Bruchle and D. Oesterhelt (1993) Photochemical conversion of the *O*-intermediate to 9-cis-retinal-containing products in bacteriorhodopsin films. *Biophys. J.* **65**, 1449–1459.
36. Gordeliy, V. I., J. Labahn, R. Moukhametzianov, R. Efremov, J. Granzin, R. Schlesinger, G. Buldt, T. Savopol, A. J. Scheidig, J. P. Klare and M. Engelhard (2002) Molecular basis of transmembrane signalling by sensory rhodopsin II-transducer complex. *Nature* **419**, 484–487.
37. Inoue, K., J. Sasaki, M. Morisaki, F. Tokunaga and M. Terazima (2004) Time-resolved detection of sensory rhodopsin II-transducer interaction. *Biophys. J.* **87**, 2587–2597.
38. Sasaki, J. and J. L. Spudich (2008) Signal transfer in haloarchaeal sensory rhodopsin-transducer complexes. *Photochem. Photobiol.* **84**, 863–868.
39. Wegener, A. A., J. P. Klare, M. Engelhard and H. J. Steinhoff (2001) Structural insights into the early steps of receptor-transducer signal transfer in archaeal phototaxis. *EMBO J.* **20**, 5312–5319.